Journal of Applied Polymer Science

Morphology and Gas-Permeation Analyses for Poly(ether sulfone)/Poly(vinyl alcohol) Electrolyte Composite Membranes in the Facilitated Transport Process

M. Esmaeili,[1] S. S. Madaeni,[1] J. Barzin[2]

[1]Membrane Research Center, Chemical Engineering Department, Razi University, Tagh Bostan, Kermanshah 67149, Iran

[2]Iran Polymer and Petrochemical Institute, Tehran 14965/115, Iran

Correspondence to: S. S. Madaeni (E-mail: smadaeni@yahoo.com)

ABSTRACT: In this article, we describe the preparation procedure of poly(ether sulfone)/poly(vinyl alcohol) (PVA) composite membranes based on film casting and evaporation methods. The morphology and operation of these membranes in the ethylene/ethane separation process were investigated. $AgNO_3$ and $AgBF_4$ salts were applied in the PVA active layer as carrier agent providers. Salt addition to PVA solution weakened the hydroxyl bond potency and fortified the position of carrier agent in the active layer structure. Scanning electron microscopy with energy-dispersive X-ray spectrometry revealed that the distribution fluctuation of carrier agents in the active layer increased with increasing salt concentration. The glass-transition and α-relaxation temperatures of the salt-containing membranes were lower than those of salt-free membranes. In addition, the polymeric structure of the salt-containing membranes showed crystallinity during the heating process at temperatures higher than 160°C. Atomic force microscopy indicated that the surface roughness of composite membranes with smoother sublayers was greater than that of other membranes. The mechanical strength of membranes containing silver nitrate salt was higher than that of the salt-free membranes. Permeation tests demonstrated an increase in the gas permeation and membrane selectivity after salt incorporation. A performance improvement in the facilitated transport mechanism was associated with increasing salt concentration. However, a higher operational pressure had an inverse impact on it. The saturation of active sites with ethylene molecules at higher pressures and the low plasticity of the created complexes in the membrane structure decreased the performance of the facilitated transport mechanism. The addition of $AgBF_4$ salt, with a lower lattice energy compared to $AgNO_3$, increased the real performance of the membranes. © 2012 Wiley Periodicals, Inc. J. Appl. Polym. Sci. 129: 1569–1585, 2013

KEYWORDS: membranes; morphology; separation techniques

Received 6 July 2012; accepted 18 October 2012; published online 18 December 2012
DOI: 10.1002/app.38749

INTRODUCTION

Poly(vinyl alcohol) (PVA) is still the most widely used membrane material. It is a hydrogel with excellent film-forming properties. Its inherent polar and hydrophilic nature creates a high tensile strength and flexibility.[1] PVA chains have stretching ability and show higher flexibility at temperatures above the glass-transition temperature (T_g; 85°C).[2] These properties make it as an attractive option in the preparation of membranes designed for a variety of water-treatment applications.[3,4] PVA is water soluble and usually exhibits high crystallinity; this arises from its high degree of intramolecular and intermolecular hydrogen-bonding interactions.[5] The embedding of PVA into membranes insoluble in water needs some degree of crosslinking.[6] Accordingly, a great deal of effort has been devoted to the modification of these membranes through the blending process. The main application of PVA membranes is in product recovery and the separation of organic compounds from one another or from water by pervaporation.[3,7] However, PVA, as a radical or auxiliary polymeric material, has been used for the preparation of facilitated transport membranes containing carrier agents.

Compared with traditional olefin recovery or separation technologies, for example, adsorption and distillation, membrane-based gas-separation technology has recently gained increasing attention. This preference refers to its distinct technical and economic advantages.[8–10] Among membrane processes, facilitated transport membranes are more attractive because both the permeability and selectivity can be improved simultaneously.[11–16] The existence of a reactive carrier in the membrane structure has made carrier-mediated transportation possible. In addition to Fickian transport, this type of transport has improved the

separation performance of facilitated transport membranes.[17] In fixed carriers containing membranes, the reaction of specific components from a feed mixture takes place in a carrier site; it then jumps to the next carrier site along the direction of the driving force through the Tarzan mechanism suggested by Cussler.[18,19]

Most applications of poly(vinyl pyrrolidone)-facilitated transport membranes in the gas-separation field have focused on CO_2 recovery.[20] Matsuyama et al.[21] prepared polyethylenimine/PVA blend membranes for the facilitated transport of CO_2. Deng et al.[1,4] and Cai et al.[19] also developed blends of PVA with poly(vinyl amine) or poly(allyl amine) for the fabrication of composite membrane based on polysulfone for the separation of CO_2/N_2 and CO_2/CH_4 mixed gases. The fixed amino groups in the poly(vinyl amine), poly(allyl amine), or polyethylenimine matrix as CO_2 carriers facilitate the transport, whereas PVA adds mechanical strength to the blend.

The utilization of nonpolymeric carrier agents in PVA structures also has been investigated in literature. Yegani et al.[22] used 2,3-diaminopropionic acid as a CO_2 carrier in the gel structure of PVA/poly(acrylic acid). Other researchers have reported the application of transient-metal salts to the PVA structure for separation purposes, especially for unsaturated compounds. Bryant et al.[23] studied the separation of a benzene/cyclohexane mixture with PVA-composite-facilitated transport membranes containing Ag(I) ions as the carrier. Shen et al.[24] conducted research using two types of cobalt salts, $Co(NO_3)_2$ and $Co(CH_3COO)_2$, in the separation of cyclohexene/cyclohexane mixtures.[24] Ho and Dalrymple[25] reported PVA casting with $AgNO_3$ for the separation of 1-butene/*n*-butane. Kim et al.[26] evaluated the selectivity and performance of PVA electrolyte membranes containing $AgSBF_6$ in propylene recovery. These studies verified that the separation properties of the noncrosslinked PVA-facilitated transport membrane in ethylene recovery are mostly ignored in the related literature.

The carrier agents, which are released from salt ionization in the PVA matrix, create complexes with the hydroxyl oxygen through the formation of carrier/—OH linkages. In this way, the carriers stabilize the membrane structure and impart new or improved properties to the polymer. Zidan[27] demonstrated that the formation of an Ag^+–PVA complex phase created another, different melting point for the PVA initial structure.[27] Shen et al.[24] concluded that cobalt cations released from cobalt salts in the membrane structure disrupted the PVA crystallinity. Moreover, the T_g of the host polymer increased after salt addition because of a restriction of the chain mobility. Clemenson et al.[28] observed the formation of silver particles in the structure of PVA films containing various amounts of $AgNO_3$ after an annealing treatment. A weakening of the hydrogen bonds in the crosslinked PVA structure was observed by Kim et al.[26] Silver salts have been used more than other transient-metal salts because of their low lattice energy and easy ion detachment. However, different efficiencies have been evaluated in membranes containing silver salts in the gas-separation process; this is caused by different coordination interactions among the silver cation and anions.[29]

In this research, composite membranes consisting of a poly(ether sulfone) (PES) support layer and a noncrosslinked PVA active layer were prepared. The chemical and physical parameters, including intercomponent interaction, ion distribution, surface roughness, mechanical strength, and T_g, were systematically determined, and the observed morphological patterns were evaluated. In addition, the ethylene separation abilities of the final composite membranes were studied in two cases. In the first step, the addition of silver nitrate with a low lattice energy and its influence on the membrane performance were analyzed. Then, a mixture of $AgNO_3$ and $AgBF_4$ was applied to increase the membrane performance. The application of mixed salts as carrier providers is a new idea that has not yet been surveyed by researchers. In addition, there has not been any report on the preparation of PES/PVA composite facilitated transport membranes for ethylene/ethane separation. A poly(dimethyl siloxane) (PDMS) layer was used on the surface of facilitated transport membranes for the first time in this study to coat the probable pinholes and increase the selectivity.

EXPERIMENTAL

Membrane Fabrication Method and Materials

PES (Ultrason E6020, weight-average molecular weight = 58,000 Da) from BASF (Germany, Schwarzheide), poly(vinyl alcohol) from Merck (Germany, Darmstadt; weight-average molecular weight = 30,000–50,000 Da), and PDMS (or Silgard) from Dow Corning Corp. were supplied as the polymeric materials for the preparation of the supportive and active layers, respectively, of the composite membranes. Dimethyl acetamide, *N*-hexane (Merck), and distilled water were used as the solvents of PES, PDMS, and PVA. Silver transient salts, $AgNO_3$ from Merck (CAS no. 7761-88-8) and $AgBF_4$ from Sigma-Aldrich, were purchased as the carrier agent producer in the membrane active-layer structure. All of the chemicals were used as they were received. The only exception was PES, which was dried further in a vacuum oven at 40°C for 24 h before use.

PES supportive flat membranes with a surface area of 20 cm^2 were fabricated via a phase-inversion method. Three solutions of PES (15, 18, and 22 wt %) in dimethyl acetamide were prepared. The solutions were agitated gently for 24 h to prepare homogeneous and bubble-free solutions. The PES flat membrane structure was formed by the casting of the solutions onto smooth glass plates and mounting the immature films in a coagulation bath (distilled water) for 10 min. After the phase-inversion process and the formation of the membrane final structures, the membranes were washed with tap water and soaked in new distilled water again for 24 h. Then, the wet membranes were placed in an oven at 40°C for 10 h to dry completely.

The active layers of the composite membranes were fabricated with different solutions of PVA+$AgNO_3$+$AgBF_4$ in distilled water through a film casting and evaporation method. Table I shows different procedures used in the preparation of the PES/PVA composite membranes. At first, uniform solutions of PVA in hot water (83°C) were prepared with a light-protected vial. After the solution was cooled, a predetermined amount of silver salt was added, and the mixture was agitated until a uniform state was reached. The concentration of PVA in all of the solutions was fixed at 10 wt %, whereas the molar ratio of monomer to silver salt was varied ([OH]/[Ag] = 9 : 1, 6 : 1, 3 : 1,

Table I. Different Procedures for the PES/PVA Composite Membrane Preparation

	Concentration of the polymer in the polymeric solution (wt %)		Thickness of layers for casting (μm)		
	PES	PVA	PES	PVA	PDMS
				[OH]/[Ag] = 9 : 1, 6 : 1, 3 : 1, and 2 : 1	
Case 1 (for general analysis)	22	10	130	10	5
	18	10	130	10	5
	15	10	130	10	5
	PES	PVA	PES	PVA	PDMS
				[OH]/([Ag_1] + [Ag_2]) = 9 : 1, 6 : 1, 3 : 1, and 2 : 1[a]	
Case 2 (for increasing selectivity)	18	10	130	10	5
	18	10	130	10	5
	18	10	130	10	5

[a][Ag_1] = $AgNO_3$ and [Ag_2] = $AgBF_4$.

and 2 : 1). The pH value of each mixture, of course, was fixed during the membrane preparation step at around 6.9, and the temperature of the laboratory was controlled at 25°C.

In the second step, the dried PES support layer was mounted on a glass plate. Its edge was sealed with Scotch tape and was coated with the prepared PVA solution via the film casting and evaporation method. The film was dried under the atmosphere for 24 h under a light-protected area. Then, it was placed in a vacuum oven at ambient temperature for 2 days to remove its water. The surface of the final membrane was coated with a thin layer of PDMS solution to decrease the number of defects and increase the membrane performance. The solution of rubbery polymer diffused in the surface cracks and restored its defects.

Characterization and Permeation Methods

The morphologies of the membranes were studied with the Fourier transform infrared (FTIR) spectroscopy–attenuated total reflection (ATR), differential scanning calorimetry (DSC), scanning electron microscopy (SEM)/EDX, and atomic force microscopy (AFM) methods. The FTIR–ATR spectra were collected for the PES/PVA–$AgNO_3$ composite membranes at room temperature with an FTIR apparatus (model Equinox 55, Germany, Ettlingen). All of the scans were signal-averaged at a resolution of 4 cm^{-1}. The spectra were taken in the region of 500–4000 cm^{-1}. The hydroxyl bond strengths before and after complexation with the silver ions were surveyed in the region of 2500–3800 cm^{-1} for clear presentation. A DSC experiment was used to analyze the thermal transitions of the PVA films with and without silver salt. The samples were heated in a Netzsch DSC differential scanning calorimeter (model Maia-200 F3, Germany, Seligenstadt) under atmospheric N_2 at a rate of 10°C/min from 20 to 220°C. AFM testing was undertaken on the surfaces of the composite membranes to investigate the effect of the sublayer on the roughness and morphology of the membrane active layers. Three-dimensional images were taken through a Dual Scope/Raster Scope AFM device (DME model C-21, Denmark, Copenhagen/Herlev) with a DS 95–50 scanner. Tapping mode was used at the cantilever resonance frequency with a probe and cantilever unit. The scan size of the membrane surface was 100 μm^2. The SEM/energy-dispersive X-ray spectrometry (EDX) analyses characterized the structure of the composite membranes and the distribution of the carrier element in the membrane active layer. The electron images were taken from the membrane cross sections with a TESCAN SEM apparatus (model VEGA II, USA, Cranberry TWP) after a 1-min focus of the probe. The mechanical strength of the composite membrane was analyzed by a Santam tensile tester machine (model STM-20, Tehran, Iran) with a crosshead speed of 1.5 mm/min. In addition, the permeation properties of the membranes were analyzed by a gas-separation system with ideal and mixed-gas separation modes. In the mixed-gas section, equal weight concentrations of ethylene and ethane gases (50 wt % of each gas) were used as the feed gases. All of the permeation tests were done at room temperature. The permeation rate of the mixed or single gas was measured by a bubble flow meter, and the separation quality was analyzed through gas chromatography. An Agilent gas chromatography apparatus (Santa Clara, CA, HP-AL/M, 19095P-M2S) with a column length of 50 mm, a diameter of 0.53 mm, and an absorbent thickness of 15 μm was used to determine the permeation rate of the gases.

The selectivity was calculated on the basis of eq. (1):

$$\alpha_{(2/1)} = (Y_2/Y_1)/(X_2/X_1) \quad (1)$$

where α is the membrane selectivity and Y and X are the demonstrators of the penetrant concentration in the permeate and feed gases, respectively. Figure 1 shows the experimental apparatus.

The bubble flow meter and mass flow controllers were purchased from Goldis (Iran) and Brooks Co. (The Netherlands, Neonstraat 3, Ede, model 5850 S), respectively.

RESULTS AND DISCUSSION

FTIR–ATR Analyses

The hydroxyl groups among the PVA chains consisted of nonbonding electrons that showed correlation with the oxygen

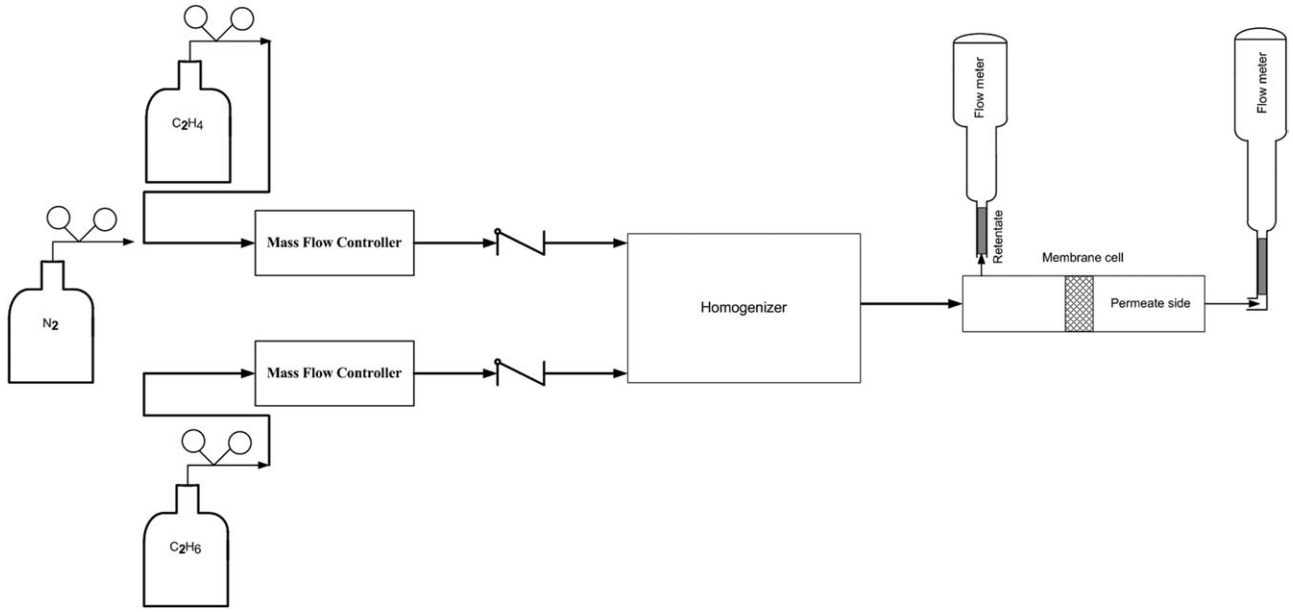

Figure 1. Schematic diagram of the gas-permeation setup.

atoms. These groups provided suitable sites for dative bond creation with the silver cations after the dissolution of silver nitrate in the PVA solution. The hydroxyl groups encountered two changes after the complexation of silver cations and hydroxyl oxygens. At first, the concentration of free hydroxyl groups decreased. The greater decrease in the concentration of free hydroxyl groups was naturally accompanied by more reaction sites of the silver cations. On the other hand, the high electronegativity of hydroxyl oxygens induced the electrons of the O—H and O—C bonding orbitals to tend toward the oxygen atom after sharing their nonbonding electrons. Therefore, the potency of the O—H and O—C bonds decreased.

To evaluate the strength variation of the main groups in the composite membranes structure with the top layer made from PVA, FTIR–ATR analyses were performed in the wave-number region of 500–4000 cm^{-1}. The main characteristic band in the PVA active layer of the PES/PVA composite membranes was a comparatively broad band around 3290 cm^{-1}. This region corresponded to the O—H stretching vibrations of the hydroxyl groups. Two small peaks were caused by the asymmetric and symmetric stretching of —CH_2 groups at approximately 2940 and 2909 cm^{-1}.[30,31] To better understand the strength vibrations of the OH and CH_2 groups, the transmittance quantity of the infrared spectrum in the composite membrane is depicted in Figure 2 in the region of 2500–3800 cm^{-1}. The lowest graph in Figure 2 corresponds to the membrane with the pure PVA active layer, which was used as a comparison reference. The minimum spectrum transmittance or maximum spectrum absorbance in the hydroxyl group of membrane surface layer was obtained at wave numbers close to 3300 cm^{-1}. As shown in the other graphs, the molar percentage of silver cations with regard to the PVA monomer was increased to 10, 14, 25, and 33% ([OH]/[Ag] = 9 : 1, 6 : 1, 3 : 1, and 2 : 1, respectively). Upon incorporation of $AgNO_3$, two types of variations in the hydroxyl group peaks were detectable in comparison to the reference graph. At first, the area under hydroxyl peak decreased; this indicated a decrease in the concentration of free hydroxyl bonds. Therefore, a higher number of hydroxyl groups was involved in the complexation with silver cations, and the active sites of the membrane structure increased for the complexation with olefin molecules.

Second, the maximum absorbance spectrum shifted from 3300 to 3234 cm^{-1} with increasing molar concentration of salt from 10 to 33%. The displacement the wave number of more powerful absorbance toward lower numbers showed that the hydroxyl groups were weakened. This was due to the lower concentration of free groups, which had a maximum amount of vibration frequency at the maximum of their absorbance. Dissolving the silver nitrate salt in the PVA solution detached the salt ions and increased the possibility of interactions between the silver cations and electron-donor groups, such as OH groups, of the PVA structure. The existence of vacant orbitals around the silver cations in the presence of nonbonding electrons in the oxygen orbital initiated interaction coordination and caused the creation of a dative bone between these orbitals. Therefore, a complex was created between oxygen and the silver cations, which had a direct effect on the vibration frequency of the OH groups. The electron cloud symmetry between oxygen and hydrogen decreased because of complex creation. Therefore, the hydroxyl bond weakened, and its maximum absorption shifted toward lower frequencies. In this way, the complex position in the membrane structure was stabilized. The duration of membrane performance increased in the permeation experiment. Hence, the reduction tendency of silver cations decreased with the consolidation of its position.

The addition of silver salt also caused variations in the CH_2 group vibration. The reduced surface area under the CH_2 peak revealed that the vibration of the theses groups weakened after the increase in the concentration of silver nitrate salt. With the formation of silver complexes and the increase in their concentrations in the PVA polymeric structure, the CH_2 groups in a

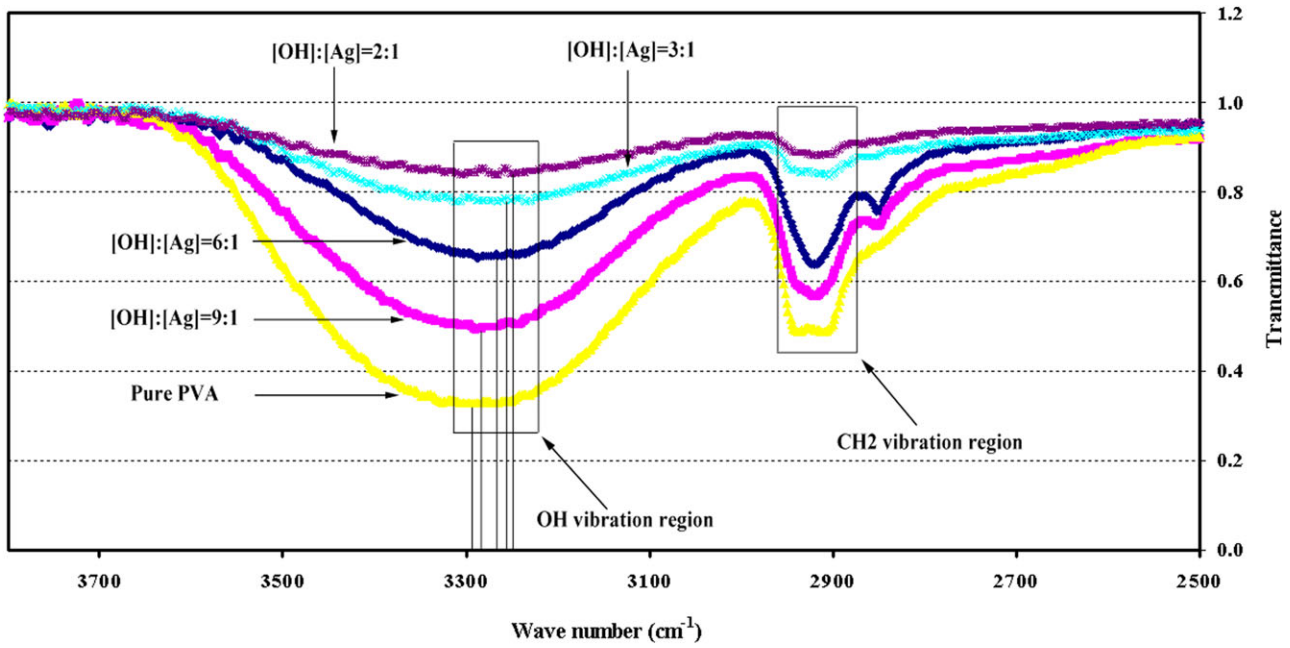

Figure 2. FTIR–ATR analyses results for hydroxyl groups in the active layer of the PES/PVA composite membranes with different molar ratios of $AgNO_3$. [Color figure can be viewed in the online issue, which is available at www.interscience.wiley.com.]

tridimensional arrangement of polymer structure encountered vibration limits between the silver and oxygen complexes or O—H and O—C bonds. As a result, the surface area under the CH_2 peak revealed a diminishing trend. However, the electronic clouds close to the oxygen atom became inclined toward it after the complexation. This is another reason for the weakening of the symmetric or asymmetric vibrations of the CH_2 groups.

SEM–EDX Experiment

The distribution of complex involved atoms in the surface and structure of facilitated transport membranes is one of the most significant and effective factors that influences the membrane structure and performance. The repartition of carrier agents affects their interactions with active sites in the membrane structure. Various factors affect the distribution of complex-forming agents. The salt type and its lattice energy and the type and concentration of the host polymer and solvent are the most important parameters in this regard. In this study, the distribution of silver nitrate salt in the PES/PVA composite membrane structure was investigated through SEM–EDX. All of the membranes had the same support layer (PES = 18 wt %), whereas the proportion of silver cations to the monomer was different ([OH]/[Ag] = 9 : 1, 6 : 1, 3 : 1, and 2 : 1). For a better demonstration of carrier distribution, the active layer of the membranes was fabricated with a relatively high thickness (nearly 15 μm).

Figures 3 and 4 show the electron images of the membrane cross section and the distribution of oxygen and silver elements

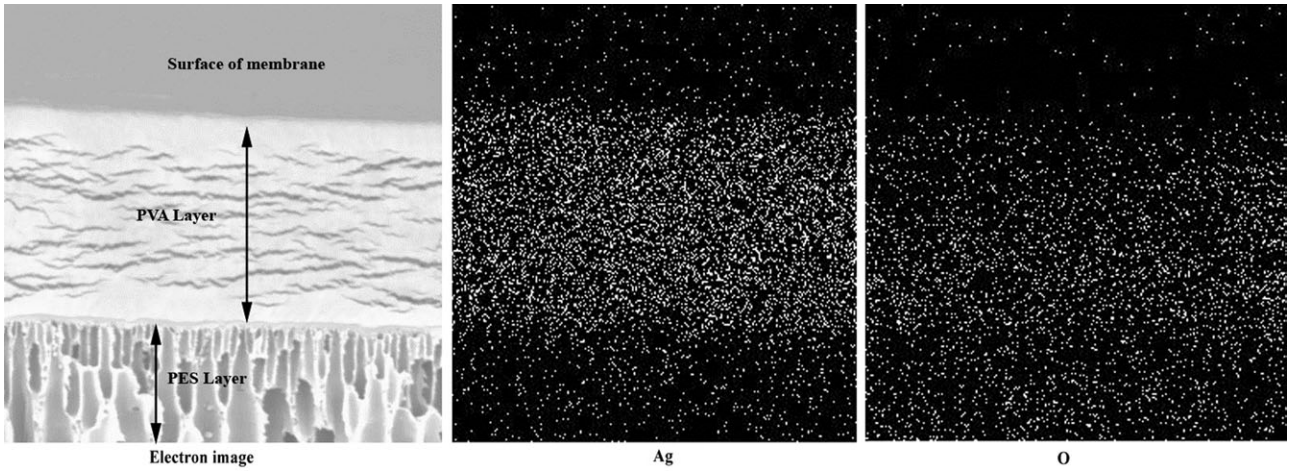

Figure 3. Electron image of the membrane cross section and the distribution of silver and oxygen elements among different layers of the PES/PVA composite membranes ([OH]/[Ag] = 9 : 1).

Applied Polymer SCIENCE

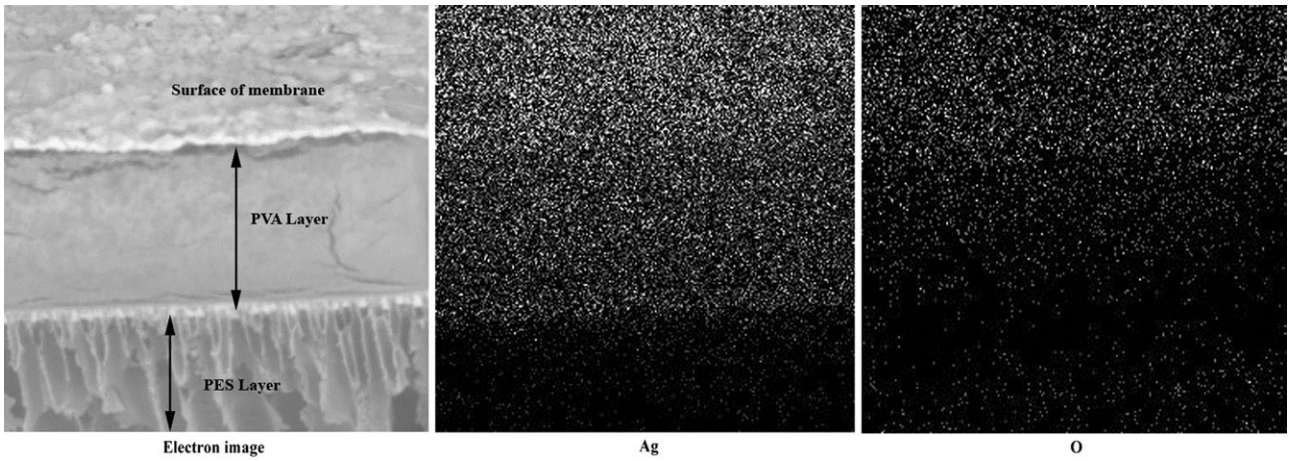

Figure 4. Electron image of the membrane cross section and the distribution of silver and oxygen elements among different layers of the PES/PVA composite membranes ([OH]/[Ag] = 2 : 1).

in the structure of the membranes. The presence of the silver element in the membrane support layer structure shown in Figures 3 and 4 justified the partial diffusion of PVA solution into the support layer. On the other hand, the presence of oxygen in this layer was due to existence of this element in the PES chains. Two changes were traceable in Figures 3 and 4 with increasing silver molar concentration from 10 to 33%. Increasing the silver concentration in the surface and structure of membrane active layer was first noted and was easily detectable. The second change was the increase in the oxygen concentration distribution in the layers above the support layer. Oxygen was a fixed part of the PVA and PES chains, and its actual concentration did not change.

Salt addition to the PVA solution was accompanied by the attachment of silver cations as carrier agents to the hydroxyl active sites of the polymer chains. Therefore, they were present in all layers above the support layer. When the salt concentration increased, the concentration of carrier agents in the polymeric layers, such as surface layer, increased, too. When the molar concentration of silver cations was less than that of the polymer active sites, there were unoccupied hydroxyl sites for cation attachment in the polymer structure. Increasing the number of complexes between silver cations and hydroxyl oxygens caused an effective presence of oxygen atoms in the active layer. This indicated a decrease in the oxygen atoms that just rested in the polymer chains or complexes without any effect on the complexation process. The number of oxygen atoms adjacent to the silver cations increased with increasing silver salt concentration. In this way, the oxygen atoms corresponding to silver cations was more assessable. The silver element, with its metallic nature, was more easily and exactly detectable by the SEM apparatus. Therefore, the detection of adjacent oxygen was easier after complex creation or an increase in the number of complexes.

For the exact evaluation of carrier agent distribution, elemental distribution in the surfaces and cross sections of the membranes are depicted in Figures 5 and 6. The vertical axes show the count of the elements, and the horizontal axes demonstrate the length of the analyzed area in Figures 3 and 4, which was equal for these two cases. In the case of the lower salt concentration

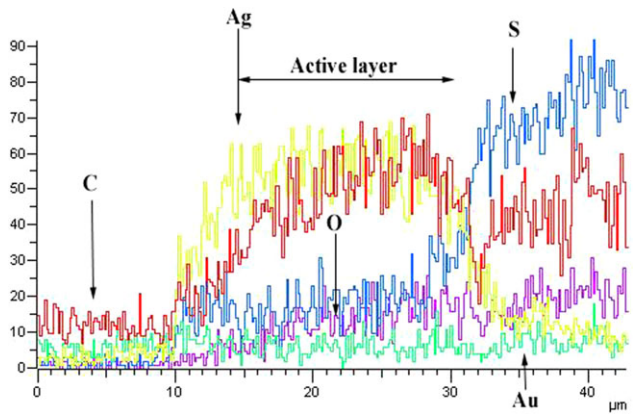

Figure 5. Fluctuations of the elemental distribution in the PES/PVA membrane layers ([OH]/[Ag] = 9 : 1). [Color figure can be viewed in the online issue, which is available at www.interscience.wiley.com.]

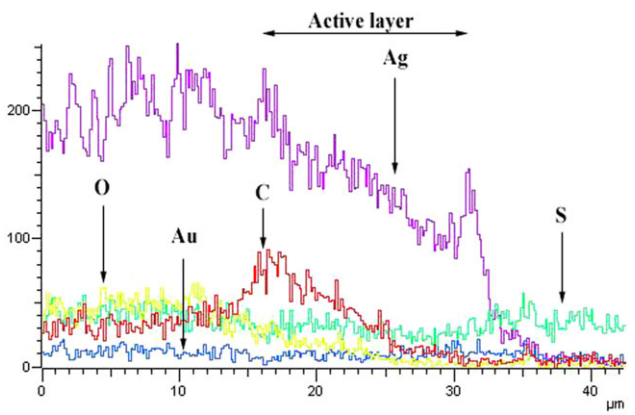

Figure 6. Fluctuations of the elemental distribution in the PES/PVA membrane layers ([OH]/[Ag] = 2 : 1). [Color figure can be viewed in the online issue, which is available at www.interscience.wiley.com.]

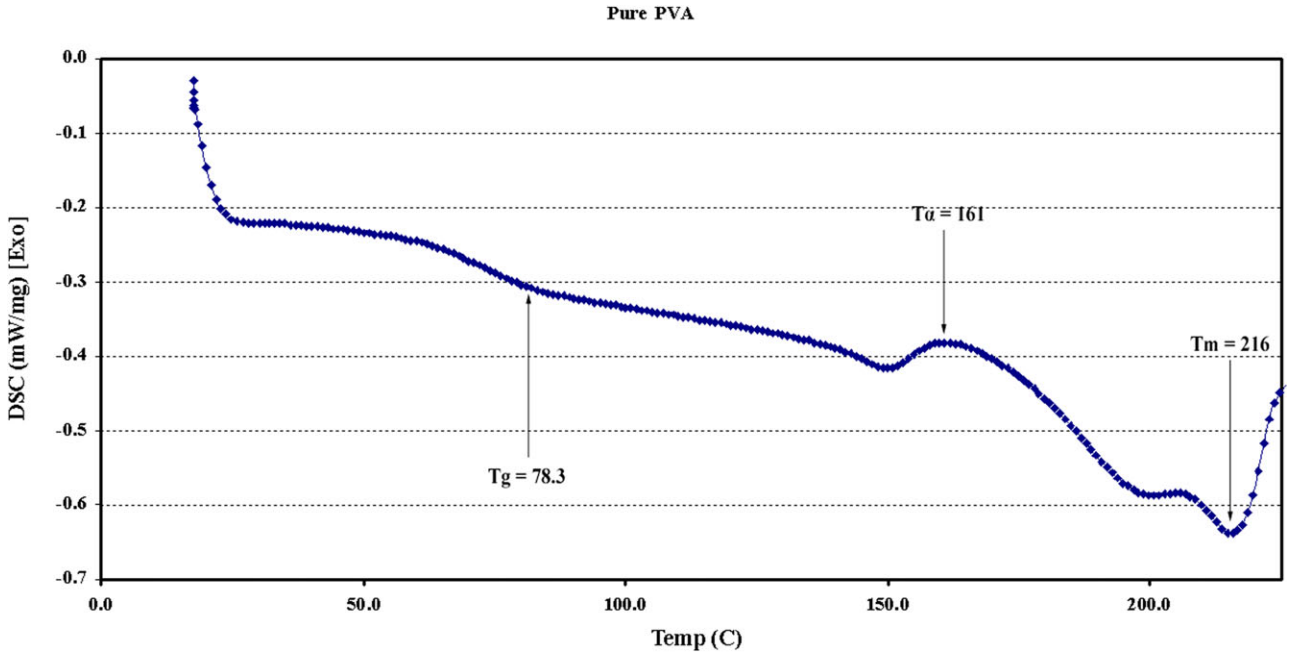

Figure 7. DSC graph of the pure PVA films with molecular weights of 30,000–50,000 Da. [Color figure can be viewed in the online issue, which is available at www.interscience.wiley.com.]

([OH]/[Ag] = 9 : 1), the distribution of carrier agent (silver cation) in the membrane active layer showed less fluctuation. With increasing salt molar concentration from 10 to 33%, the dispensation uniformity of the silver element among the membrane layers decreased. The count ranges of silver element in the active layer sections of Figures 5 and 6 were between 30 and 70 and 80 and 230, respectively. The difference was due to a reduction in the solvent potency for opening the polymer chains and dissolving the silver salt. The cations and polymer active sites could not interact with each other effectively, and the aggregation of silver cations occurred. Therefore, the homogeneity of carrier distribution among polymer chains decreased with increasing salt concentration. The count ranges of silver element in the surfaces and support layers of these membranes were lower than the active layer ranges. The detected sulfur and gold between the layers was due to presence of sulfur in the PES composition and the gold coating from the SEM experiment, respectively. In addition, the higher fluctuations of oxygen distribution with higher silver concentrations are observable more exactly in Figures 5 and 6. The undesirable and heterogeneous distribution of silver cations and, therefore, the interaction forces between them and the oxygen atoms explained this result. The oxygen element tended to move to positions with higher concentrations of silver cations.

DSC Analyses

The thermal behavior of polymers used in the preparation of facilitated transport membranes changes with transient salt addition to the polymeric solution. This trait evaluation shows the effects of additives with various concentrations and reveals the membranes structural changes. The examination of the thermal behavior of polymers with intermingled amorphous and crystalline phases is more difficult than that of polymers with highly crystalline or amorphous natures. PVA is a polymer with coexistent amorphous and crystalline features; these depend on its grade and molecular weight and make its thermal evaluation difficult. For example, Zidan[27] encountered four transition regions at 78, 125, 170, and 192°C during the heating process of PVA. In this study, different PVA films with various molar concentrations of $AgNO_3$ (0, 10, 14, 25, and 33) were heated with a DSC apparatus in the temperature range 20–220°C. Figure 7 shows the thermal analyses graph of the pure PVA film. The resulting graphs for other films are depicted in two separate figures because of the expanded variations region of DSC (Figures 8 and 9). One was in the temperature region of 20–150°C, and the other was in the region 150–220°C. The T_g, the α-relaxation temperature (T_α), and melting point values for pure PVA were equal to 78.3, 161 and 216°C, respectively. The thermal graph of pure PVA was obtained after the heating and cooling cycle. This solvent (water) in the polymer chains vaporized during the heating phase, and so the solvent evaporation peak happened near 100°C, which is not shown in Figure 7. However, the thermal analyses of the films consisted of $AgNO_3$ salt, and their results are depicted in Figure 8; this was done only in the heating phase, and a relatively wide endothermic peak for water evaporation was detectable in the graphs.

A comparison of Figures 7 and 8 revealed that the T_g of PVA decreased because of a gradual increase in the silver nitrate salt concentration in the film structure. The T_g, T_∞, and crystallization temperature (T_c) values of the films are shown in Figures 8 and 9. The T_g reduction was due to the disordered increase of the polymer matrix after the salt concentration increase, which caused a higher intertwining of polymer chains. Undoubtedly, the complexation between the salt cations and the active sites of the polymer structure led to crosslink formation. Disorder in

Applied Polymer SCIENCE

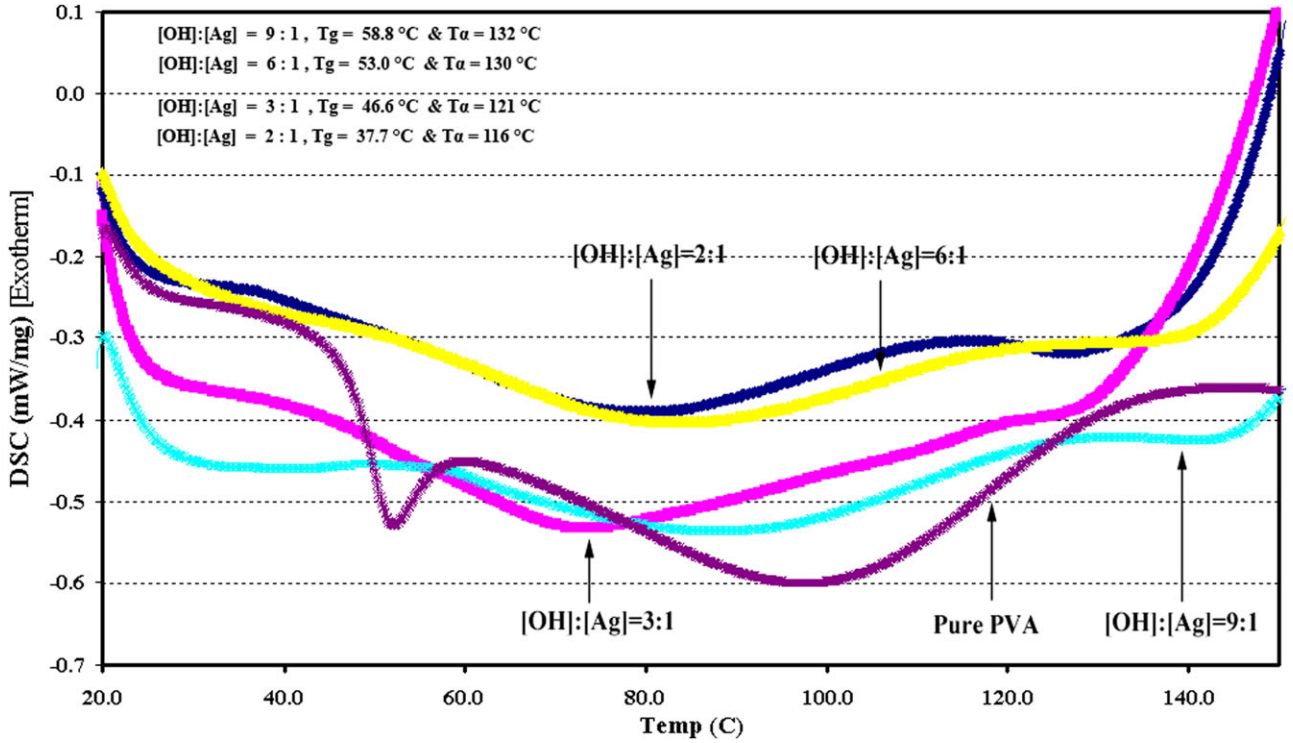

Figure 8. DSC graphs of the PVA films containing silver nitrate in the region of 20–150°C. [Color figure can be viewed in the online issue, which is available at www.interscience.wiley.com.]

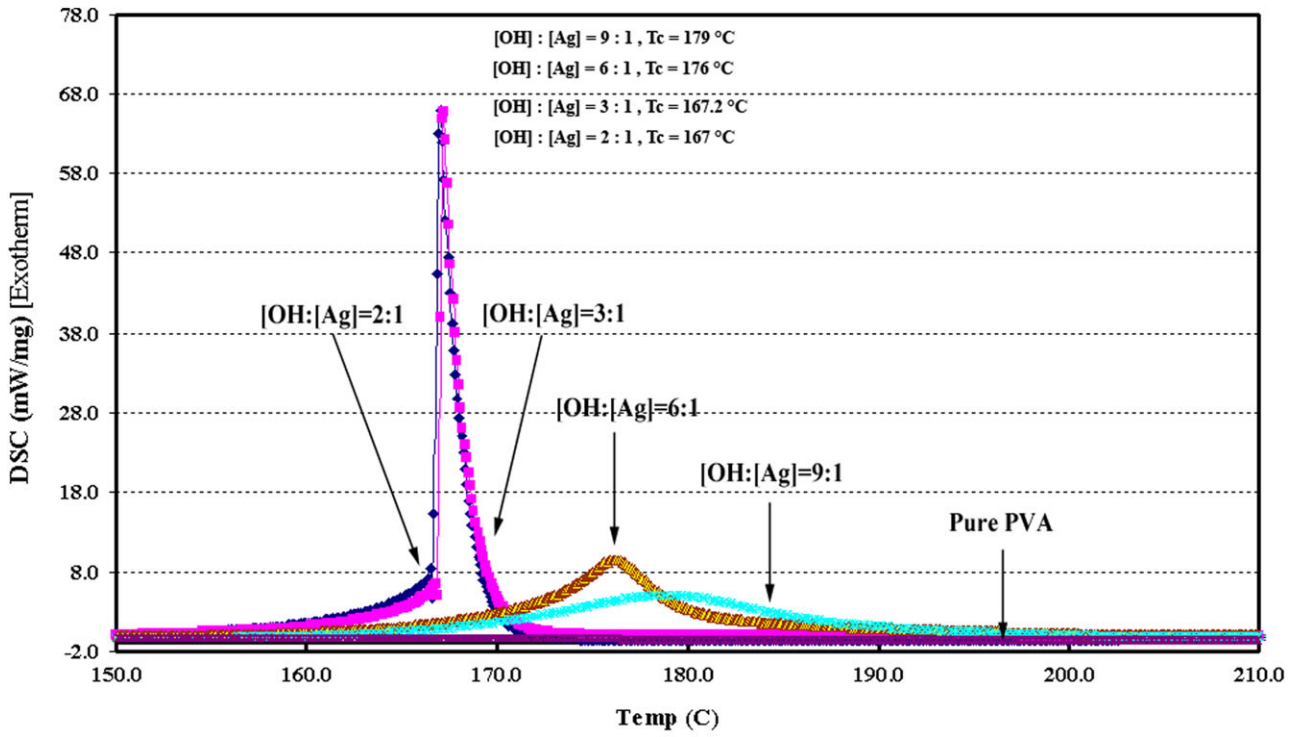

Figure 9. DSC graphs of the silver nitrate containing PVA films in the region of 150–220°C. [Color figure can be viewed in the online issue, which is available at www.interscience.wiley.com.]

the PVA chains, however, had a more pronounced effect on the T_g variations. A collation of Figure 8 with the graph related to the heating step of the pure PVA film demonstrated that the endothermic peak of water evaporation shifted to lower temperatures. The change was due to amorphism and a free volume increase in the polymer structure. Therefore, the solvent evaporated and exited the film more easily.

T_α changed with the addition of $AgNO_3$ to the film structure. A comparison of Figures 7 and 8 revealed that the small endothermic peak of T_α shifted toward temperatures below 161°C after the salt addition. T_α is related to a kind of polymer chain relaxation and led to a small increase in the chain order and the emergence of a slight crystallinity in the polymer structure. Subsequent to the addition of salt and complexation, the polymer chains found a more ordered arrangement, which caused an improvement in the chain order after they were loosened. The achievement of a semiordered chains arrangement was possible in lower temperatures with increasing complex number and electrostatic interactions in the polymer structure.

When the polymeric film heating process was continued after T_α was reached, the electrostatic forces with a maximum impression in the polymer chains led to the formation of a crystalline structure at a certain temperature. More interactions with higher salt concentrations increased the crystallinity. The creation of a crystalline and ordered arrangement led to the exothermic peak emergence shown in Figure 9. T_c, like T_α, shifted toward lower temperatures with higher salt concentrations. The area under the T_α peak showed the crystallization quantity, which was higher in polymers with higher salt concentrations. After the polymeric film heating process, the melting peak of the silver-salt-containing films was not observed up to 220°C because of the formation of a semicrystalline and ordered structure. This meant that the salt addition increased the melting temperature (T_m) of the PVA film.

Mechanical Strength

The mechanical strength of facilitated transport membranes varies with the incorporation of transient-metal salts. The type and concentration of the applied salt and the polymer are the most important factors affecting the mechanical strength of the membranes. The variation trend of the membrane mechanical strength after the increase in the salt concentration depends on the initial crystallinity of the host polymer. Disorder increases in the membrane structure and crosslinking happens among the polymer chains with the creation of electrostatic interactions. These factors affect the mechanical strength of the membranes in two different ways. The increase in amorphism means a higher free volume in the polymer structure; this leads to an enhancement in the polymer elasticity against applied stress. The creation of crosslinking increases the crystallinity of the polymer structure and keeps the polymer chains close to each other with a higher strength. In this way, the elasticity of the polymer structure and the membrane mechanical strength decrease. Consequently, the membrane becomes brittle. To evaluate the effects of these two factors on the mechanical strength of the PES/PVA composite membranes, tensile strength analyses were performed, and the related results are depicted in

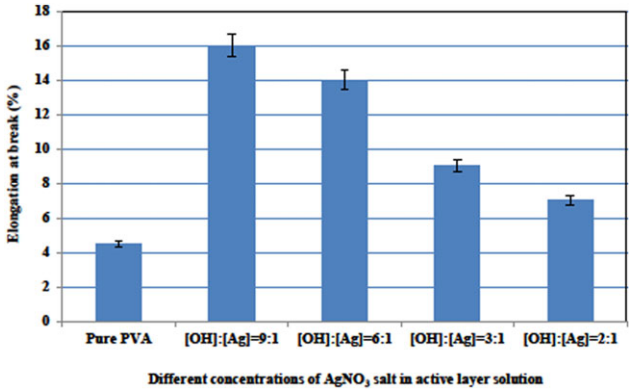

Figure 10. Variation of the mechanical strength of the PES/PVA composite membranes versus different concentrations of $AgNO_3$ salt in the active layer solution. [Color figure can be viewed in the online issue, which is available at www.interscience.wiley.com.]

Figure 10. The prepared membranes were cut into equal sizes of 1.5 × 4 cm^2 and were placed between two arms of a Santam machine one by one; this applied 6 kg of force for stretching the membranes. The samples had the same thickness of 65 μm for exact evaluation of salt concentration on the membrane mechanical strength.

A comparison of the mechanical strength of the membranes containing silver salt with that of salt-free membranes revealed that the incorporation of $AgNO_3$ salt increased the mechanical strength of the PES/PVA membrane. The maximum elongation at break increased from 4.5 to 16% with increasing salt concentration to 10 mol % ([OH]/[Ag] = 9 : 1). The reason was the disordered arrangement and complex formation between hydroxyl active sites and silver cations after ion distribution. However, the mechanical strength of the PVA matrix in the membranes containing $AgNO_3$ salt showed a different trend with increasing salt concentration. Higher salt concentrations were accompanied by improvements in the crosslinking formation, crystallinity effects, and a weakening of amorphism. In this way, the descending trend of the membrane mechanical strength was observable compared to that of the membrane including the lowest salt concentration. The resistance of the membrane structure against stretching forces decreased with decreasing free volume of the polymer matrix. The elastic form of the membrane structure shifted toward a fragile state after crosslinking formation. Therefore, the endurance of the membrane against the applied force decreased, and the elongation at break decreased, as shown in Figure 10. However, salt incorporation at the highest concentration could not neutralize the amorphism effect, and so the mechanical strength of the PES/PVA membrane with the highest salt concentration was higher than that of the membrane without salt.

AFM Experiment

The surface characteristics of the support layer are factors that affect the quality of the active layer created on the support membrane. The roughness degree of each surface affects the smoothness or roughness of its top layer. Decreasing the roughness of the support layer will decrease the roughness of its top

Applied Polymer SCIENCE

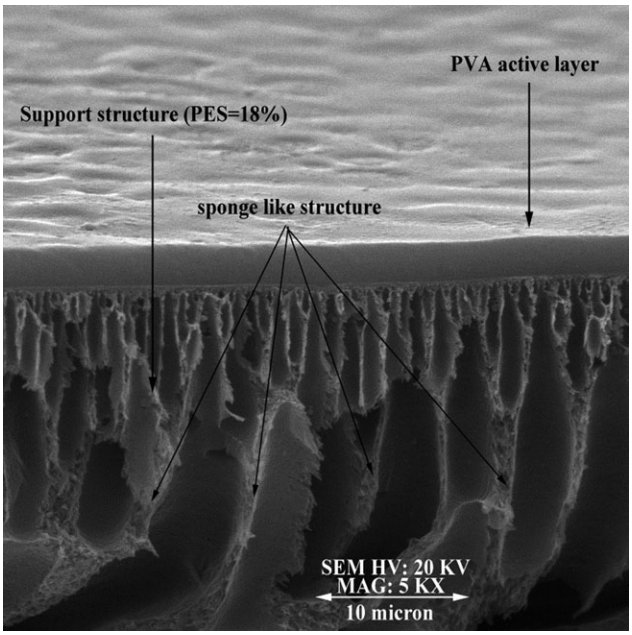

Figure 11. SEM image of the cross section of the PES/PVA composite membrane without a PDMS layer (PES = 18 wt %).

layer, which is created through the casting of a pure polymeric solution. However, if the created layer on the surface contains complexing agents, the top-layer roughness will vary in another way. The complexing agents on the surface with low porosity will distribute more homogeneously in polymer chains. Therefore, the active sites of the polymer structure and complexing agents can absorb each other with interactions that are more powerful. These electrostatic and distributed forces cause the polymer chains to encounter more bending and variation. In this way, the created layer on the surface shows more roughness. In this survey, solutions of pure PVA and PVA with two different concentrations of $AgNO_3$ salt were used in the surface roughness evaluation of a polymeric film containing complexing agents. First, the cross section of the salt-free PVA/PES composite membranes, which were fabricated on the basis of the phase-inversion method (PES 18 and 22%), are depicted in Figures 11 and 12. The thickness of the layers and the existence of differences between the surface layers is detectable in these figures. The PVA active layer, which was created on the surface of PES with a concentration of 22 wt %, showed a smoother surface.

Figure 13 depicts the AFM images of the composite membrane surfaces in which the support layer was made of PES with two different concentrations: 18 and 22 wt %. The reported numbers in this figure are related to S_y. This parameter showed the height difference between the highest peak and the lowest valley as a surface roughness sign. As shown in Figure 13(a,b), the created active layer was completely devoid of $AgNO_3$ salt. The created active layer had less roughness in the case of PES with a concentration of 22 wt %. Because of the structural compactness of the support membrane with the increasing PES concentration from 18 to 22 wt %, the surface layers of the support membrane had less porosity and more compactness at higher PES concentrations. Consequently, a smoother support membrane surface was obtained with a higher polymer concentration. The active layer created on a smoother surface has less porosity and roughness.[32] Nevertheless, a comparison of Figure 13(c) with Figure 13(d–f), which are related to the $AgNO_3$-salt-containing polymeric layers, revealed different trends. The salt concentrations of the active layer solution were 0.1 ([OH]/[Ag] = 9 : 1) in Figure 13(c,d) and 0.33 ([OH]/[Ag] = 2 : 1) in Figure 13(e,f). In each of these two cases, the roughness of the surface layer created on a more compact support layer [Figures 13(d,f)] was greater than that of the other layer [Figure 13(c,e)]. The result was explained by a more homogeneous distribution of the complexing agents, which were created on the smoother support layers. Homogeneous distribution caused the interaction forces among the atoms to be dispersed throughout the active layer structure and to reach its maximum effect. Moreover, a comparison of Figure 13(c) with Figure 13(e–f), which are related to the active layers created from the casting of the PVA solutions with different concentrations of silver salt on the same support membrane, revealed their accurate trends. Studies have shown that the concentration addition of complexing agents is accompanied by increases in both the internal interactions and the roughness of the active layer.[33] In this way, the application of facilitated transport composite membranes with higher surface roughnesses (in the case of the same support layer) helped to better separate olefin molecules because of a better distribution of complexion agents.

Further evaluation was undertaken with DME/SPM software (Copenhagen/Herlev, Denmark) to calculate the surface roughness parameters, and these results are shown in Figure 13. The value of the mean height difference between the highest peak and the deepest valley (S_z) was a little bit lower than S_y. However, their variation trends were similar, and the evaluation of the S_z variation trends confirmed the preceding results. The S_{ds} parameter explains the number of peaks per unit of analyzed area. Because of the similarity of the S_y and S_z parameters, the lower distance between adjacent peaks could be assigned to a higher S_{ds} value. In this way, the surface was very smooth when

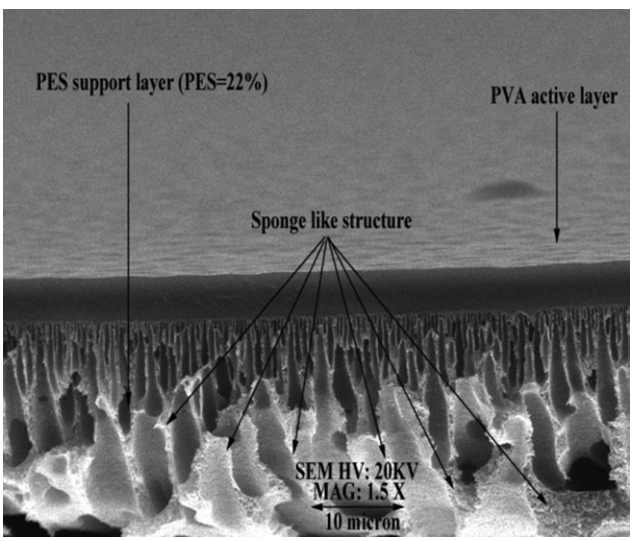

Figure 12. SEM image of the cross section of the PES/PVA composite membrane without a PDMS layer (PES = 22 wt %).

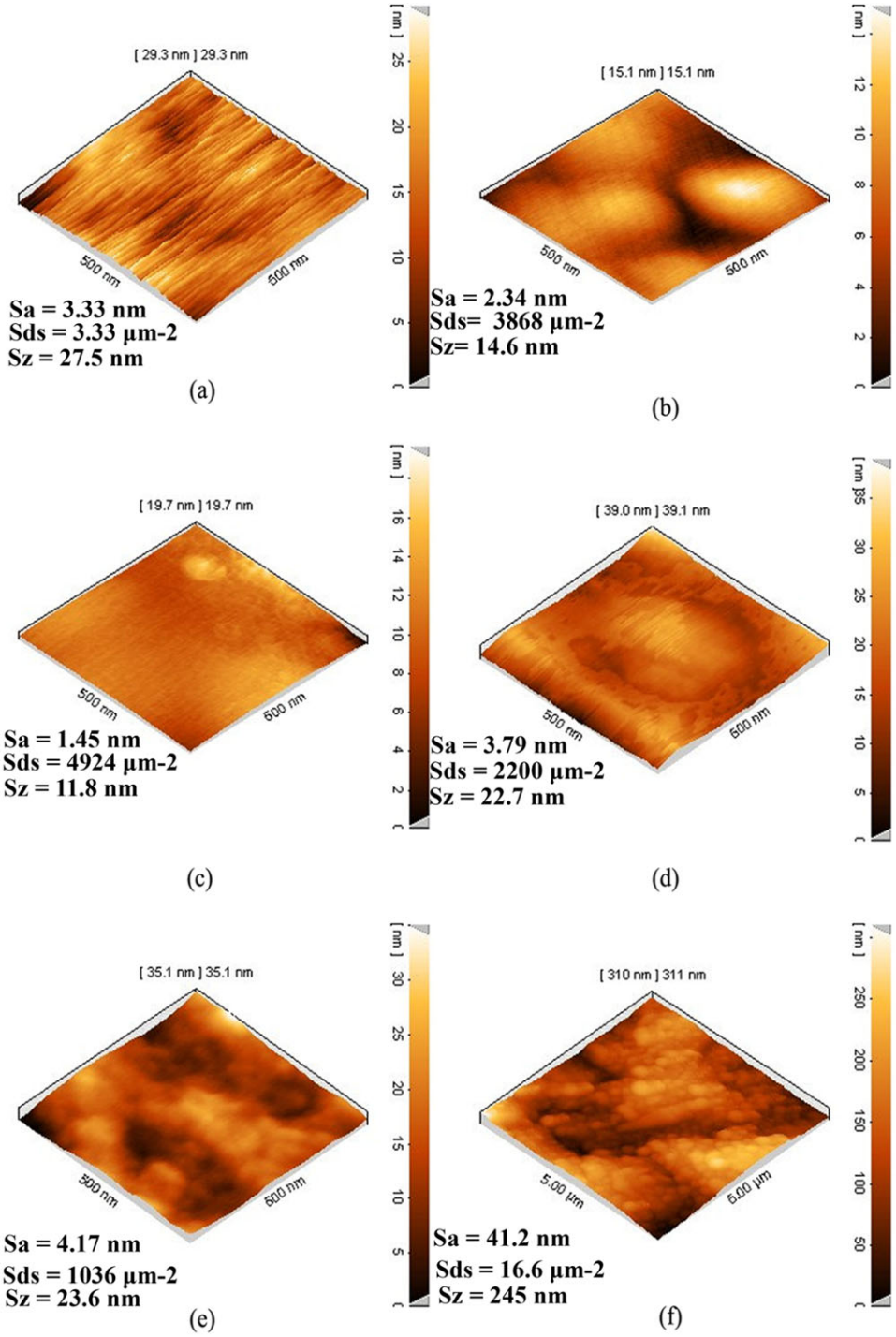

Figure 13. AFM images of the composite membranes surfaces prepared from PVA and $AgNO_3$ in the active layer: (a) active layer without salt and an 18 wt % PES concentration in the support layer, (b) active layer without salt and a 22 wt % PES concentration in the support layer, (c) 18 wt % PES concentration in the support layer and in the active layer ([OH]/[Ag] = 9 : 1), (d) 22 wt % PES concentration in the support layer and in the active layer ([OH]/[Ag] = 9 : 1), (e) 18 wt % PES concentration in the support layer and in the active layer ([OH]/[Ag] = 2 : 1), and (f) 22 wt % PES concentration in the support layer and in the active layer ([OH]/[Ag] = 2 : 1). [Color figure can be viewed in the online issue, which is available at www.interscience.wiley.com.]

there were equal-sized peaks, and their intervals were placed in the possible maximum and minimum values, respectively. The variations trends of S_{ds}, however, confirmed the membrane surface changes.

The mean pore size and distribution of pores in the active layer surface of the PES/PVA composite membranes were affected after salt incorporation. These parameters, which had an important role to play in membrane performance, could be evaluated

Applied Polymer SCIENCE

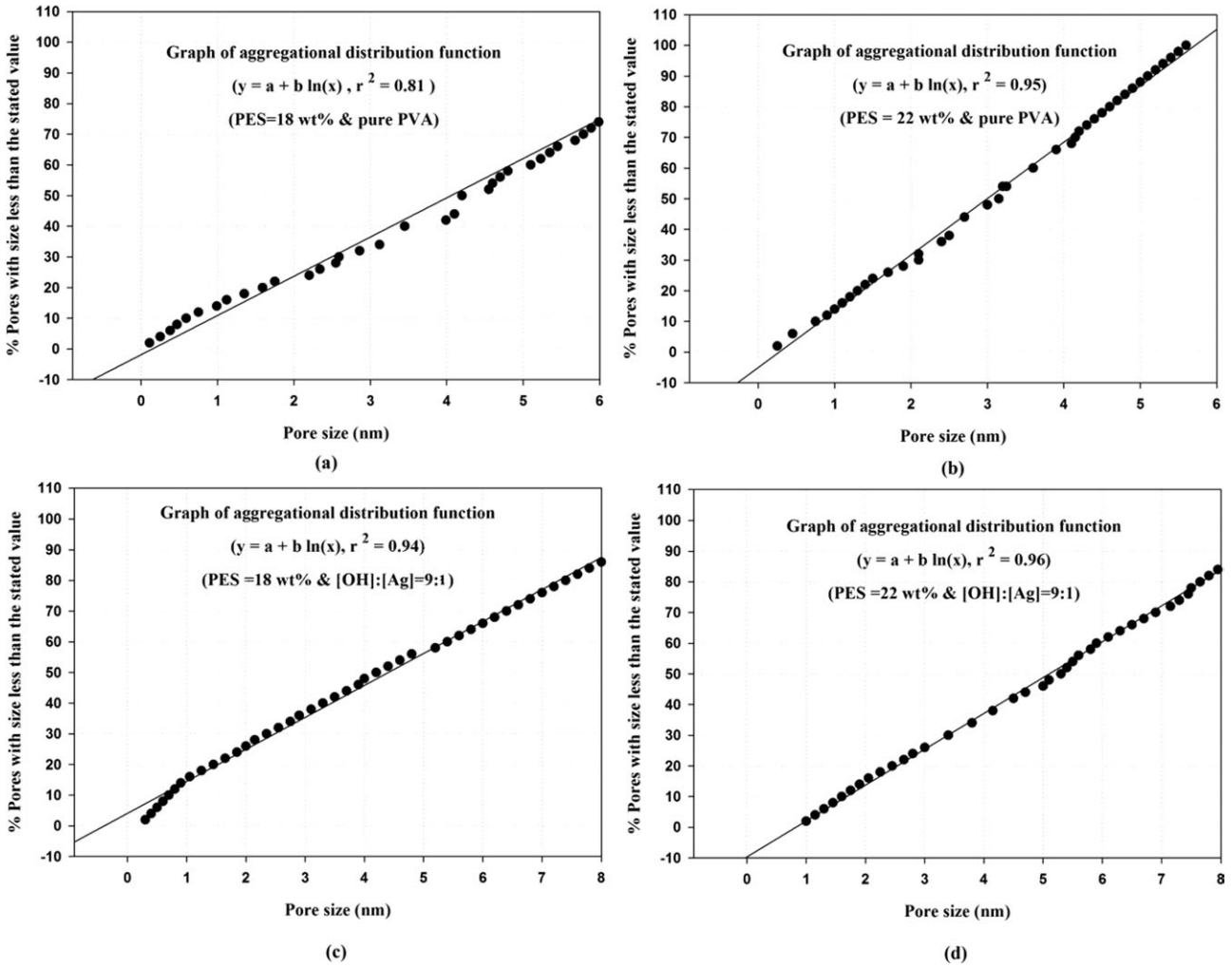

Figure 14. Pore size distribution in the active layer: (a) PES/PVA composite membrane with a PES concentration of 18 wt % and pure PVA, (b) PES/PVA composite membrane with a support concentration of 22 wt % and pure PVA, (c) 18 wt % PES concentration in the support layer and in the active layer ([OH]/[Ag] = 9 : 1), and (d) 22 wt % PES concentration in the support layer and in the active layer ([OH]/[Ag] = 9 : 1).

through different methods. Analysis of the AFM images was one of these methods and was based on the appraisal of the linear profiles of each image.[34] The roughness of the support layer, the potency of interconnections among the cations and electron-donor groups of the polymer structure, the type of silver cations, and the salt concentration were some of the main factors that influenced the mean pore size of the active layer. In this research, four types of composite membranes were nominated for pore size investigation. Composite membranes with PES concentrations of 18 and 22 wt %, which were free from silver cations, were selected to study the effect of support concentration. However, composite membranes with the same molar concentration of [OH]/[Ag] (9 : 1) were selected to assess the effect of the salt concentration. Different AFM images of these membranes were surveyed, and the size of the pores was depicted versus their amplitude in the graphs of the aggregation distribution function. SigmaPlot software (Systat Inc., Point Richmond, CA 94804-2028, USA) was applied to analyze the pore size distribution and determine the mean pore size, and the related results are shown in Figure 14. The mean pore size was obtained from the point with an amplitude of 50% when the regression of these parameters followed the normal logarithmic model.

The composite membrane with a support concentration of 18 wt % had less surface roughness than the other membrane (support concentration = 22 wt %), which caused the creation of a more smooth active layer on the membrane. A higher surface roughness was an acceptable reason for the dispersal of its pore size. Fifty percent of the pores had a size of less than 4.13 nm according to Figure 14(a), whereas the mean pore size of the membrane, shown in Figure 14(b), was 3.0 nm. However, the regression coefficient of Figure 14(b) was higher than that of Figure 14(a). In this way, the composite membrane with a PES concentration of 22 wt % demonstrated a higher resistance against the permeation of gas molecules. On the other hand, the mean pore size of the membranes containing silver salt [Figure 14(c,d)] was higher than that of the membranes without salt. The mean pore sizes of the membrane containing a silver molar concentration of [OH]/[Ag] of 9 : 1 on the support concentrations of 18 and 22 wt % were 4.3 and 5.35, respectively.

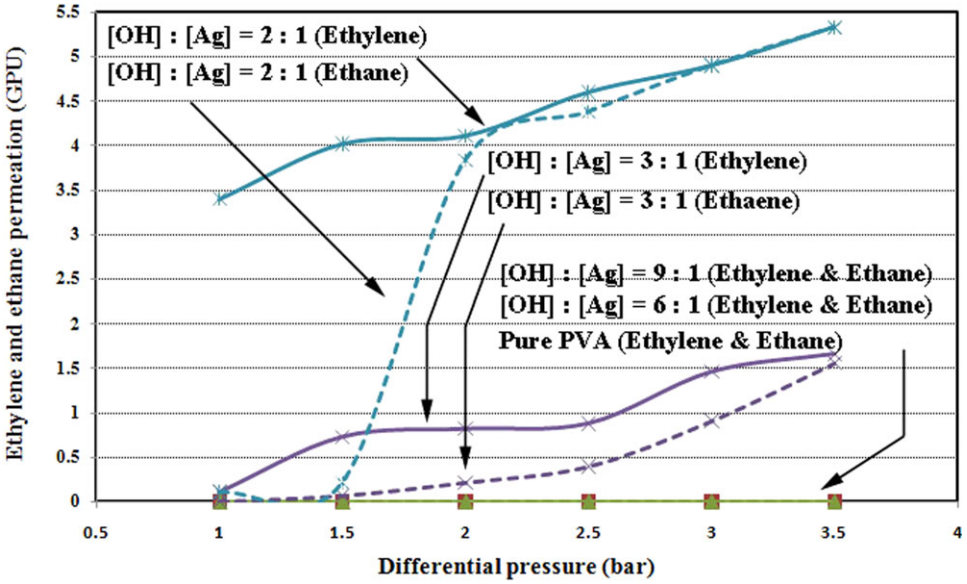

Figure 15. Ethylene and ethane permeation through the PES/PVA/PDMS composite membranes containing different concentrations of silver nitrate (PES = 18 wt %). [Color figure can be viewed in the online issue, which is available at www.interscience.wiley.com.]

The maximum size of pores in the surface of membranes containing silver salt was about 8.0 nm, that is, higher than the size of pores in the membranes without salt (ca. 6 nm). The creation of interaction forces among the silver cations and electron donor groups of the polymer structure was the reason for the increase in size. The existence of interactions in the active layer with lower roughness (22 wt %) created pores with a higher size. Therefore, the application of these PES/PVA facilitated transport membranes with lower PES concentrations for gas separation will promise better separation performance.

Gas-Separation Performance

The permeation and separation properties of solid polymer electrolyte membranes manufactured from PES, PVA, $AgNO_3$, and $AgBF_4$ were studied in this experiment. Various concentrations and thicknesses of PES and PVA solutions were used in the preparation of the support and active layers of the membranes, as shown in Table I. The PES concentration in the support layer affected the mechanical strength and flux of the membrane, whereas the PVA and silver salt concentration influenced the membrane selectivity. The membranes were tested in the pressure region of 1–3.5 barg. The results show that the composite membranes prepared from 22 wt % PES had very low and undetectable ethylene and ethane permeabilities. On the other hand, the membranes produced from 15 wt % PES did not show any reportable selectivity. The permeation properties of the membranes prepared from 18 wt % PES showed a reasonable trend, and these results are shown in Figures 15 and 16.

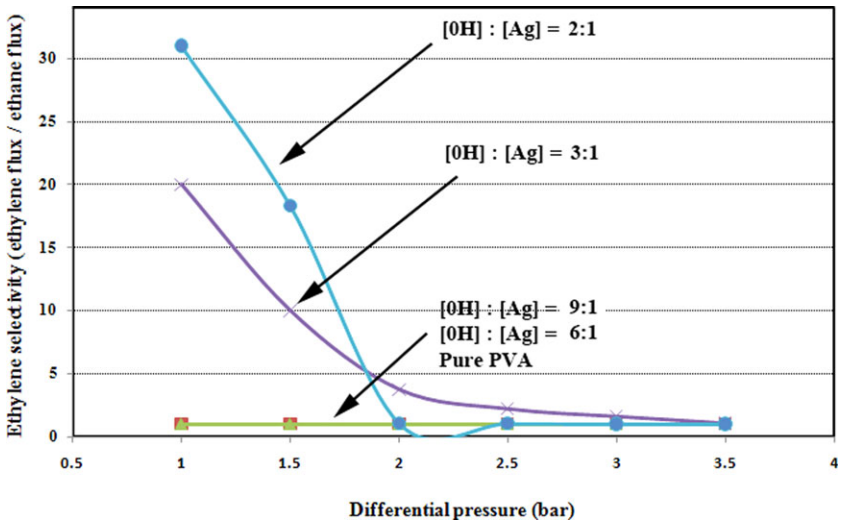

Figure 16. Ideal ethylene selectivity in the PES/PVA/PDMS composite membrane containing different concentrations of silver nitrate (PES = 18 wt %). [Color figure can be viewed in the online issue, which is available at www.interscience.wiley.com.]

The effects of the concentration of salt, as the membrane carrier agent, and the operational pressure on the membrane permeation properties are shown in Figures 15 and 16. The number of active sites increased, and the effective distance between them decreased with increasing silver nitrate concentration. The salt concentration enhancement augmented the number of complexes between the silver cations and the polymer hydroxyl groups. Therefore, the number of membrane active sites increased, and the possibility of ethylene absorption and transportation was enhanced. The penetrated ethylene molecules could be transferred more easily to the other side of the membrane through a hopping mechanism between the active sites. On the other hand, the number and concentration of carrier agents on the membrane surface layers increased with increasing molar concentration of silver salt from 0.0 to 33%. There were greater tendencies toward the attraction of ethylene from the gas stream on the membrane surface and transportation through the membrane structure. This indicated the higher potential for the facilitated transport mechanism. Figure 15 shows the ethylene flux increment due to the increase in the silver salt concentration and the strengthening of the facilitated transport mechanism. An increase in the crystallinity of the membrane structures containing a higher salt concentration caused the facilitation of the transportation and diffusion of gas molecules between active sites. In this way, the permeation of ethylene and ethane molecules increased at each pressure with increasing salt concentration because of the strengthening the diffusion mechanism. On the other hand, the flux of the permeate stream increased with increasing operational pressure as the permeation driving force. The effect of the pressure variation on the membrane permeation properties was not considerable at salt molar concentrations below 25 wt % ([OH]/[Ag] = 3 : 1). This indicated an insufficient concentration of carrier agents on the surface and structure of the membranes for ethylene adsorption and transportation.

The transmission of ethylene molecules through the structure of the facilitated transport membranes was affected by both a diffusion mechanism and a hopping mechanism. Nevertheless, the similarity of the molecular sizes of ethylene and ethane limited the effect of the diffusion mechanism on the variation of membrane selectivity. The membrane active sites had a greater effect on the increase in selectivity at low pressures. At high pressures, the permeation rate of gases through the diffusion mechanism was greater than that through the facilitated transport mechanism, which decreased the membrane selectivity. The pressure increase was accompanied by an increase in the ethylene molecule concentration in the membrane structure. Therefore, the active sites were saturated with ethylene molecules. The existence of high electrostatic forces among the silver cations and the hydroxyl groups of the membrane structure saturated the active sites with ethylene molecules. The OH—Ag^+ complexes showed less plasticity between the silver cations and other agent groups such as carbonyl bonds compared the created complexes. These complexes showed less of a tendency toward ethylene molecule abandonment.[21,22] The attracted ethylene molecules encountered transferring difficulty toward other active sites when the complex had less elasticity. In this way, the number of unbound gas molecules diminished in relation to the molecules diffused into polymeric layers, and the saturation of active sites occurred. However, the effect of the diffusion mechanism increased at higher pressures. Therefore, the performance of the facilitated transport mechanism and membrane selectivity decreased with increasing pressure.

The increase in the salt concentration led to an increase in the amorphism and free volume of the polymer structure; this caused a higher permeation of gas molecules by the diffusion mechanism. Consequently, the selectivity of the membranes decreased with increasing operational pressure for each salt concentration. This phenomenon decreased the selectivity to 1.0 at pressures above 2.0 barg. The maximum selectivity of 31.7 was obtained from the composite membrane containing a 0.33 mol % concentration of silver nitrate salt at 1.0 barg. The ethylene permeation rate at this point was 3.4 GPU; this increased with increasing operational pressure. The higher potential of the facilitated transport mechanism at higher salt concentrations in the membrane structures was the reason for the higher ethylene permeation and higher ethylene selectivity in these membranes. The permeation rates of ethylene and ethane at salt molar concentrations below 0.25 ([OH]/[Ag] = 3 : 1) were near zero. The dense structure of the membrane and the low concentration of carrier agents were the reasons for the undetectable permeation rate of the gases.

The separation capability of silver carrier agents decreased when the membranes were exposed to reducing agents, such as UV light or olefinic gases. This problem will limit the application of these membranes for industrial purposes or long-term use. In this section, the composite membranes were exposed to a pure ethylene gas stream for 8 h at a pressure of 3.5 barg. Then, we performed the pure and mixed gas-permeation analyses on them; the results are depicted in Figures 17 and 18. Electron attraction from olefinic molecules toward silver cations accelerated the reduction process of the carrier agents and the formation of silver metal particles in the membrane structure. In this way, the possitive surface charge of the membranes containing silver cations decreased. Consequently, the number of active sites on the surface and the structure of membranes decreased, and the potential for the facilitated transport mechanism for transferring olefinic molecules decreased. On the other hand, the amorphism degree of the membrane structure decreased after the OH/Ag^+ complexes collapsed. Therefore, the elasticity of the membrane structure and the potential of the diffusion mechanism for gas penetration decreased. These phenomena weakened the selectivity of ethylene over ethane and the permeation rate of gases through the active layer structure. The maximum selectivity of the composite membranes after ethylene exposure time was 12; this was obtained from the membrane containing the highest salt concentration ([OH]/[Ag] = 2 : 1). The ethylene and ethane permeation rates at the minimum operational pressure were 2.52 and 0.21 GPU, respectively. The selectivity of these membrane was eqaul to 1.0 at pressures higher than 2.0 barg. The variation trends of the permeation and selectivity of the membrane before and after the exposure process were the same. Nevertheless, the values of these parameters were decreased after the exposuring time passed.

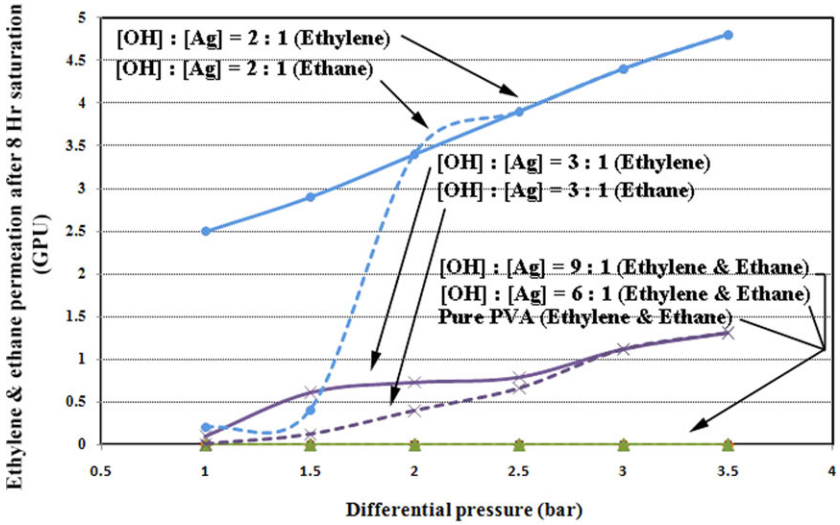

Figure 17. Ethylene and ethane permeation through the PES/PVA/PDMS composite membranes containing different concentrations of silver nitrate after 8 h of saturation with an ethylene stream at 3.5 barg (PES = 18 wt %). [Color figure can be viewed in the online issue, which is available at www.interscience.wiley.com.]

The existence of both ethylene and ethane molecules in the feed gas reduced the probability of an effective confluence between the ethylene molecules and surface-active sites. The partial pressure of each gas in the mixed-gas-permeation analyses was lower than that in the pure case. Therefore, the partial concentration of ethylene gas in the vicinity of the membrane surface was lower than in any other case. However, ethylne and ethane permeation occured synchronously through the diffusion mechanism. In this way, the selectivity of the PES/PVA/PDMS composite membrane for ethylene molecules decreased when both gases were used together in the gas-permeation analyses. The mixed gas-permeation results are depicted in Figure 19. The maximum real selectivity was 6.8 at the lowest operational pressure. The pressure boundry in which the membrane containing the highest salt concentration ([OH]/[Ag] = 2 : 1) lost its selectivity completely shifted from 2.0 to 2.5 barg. The decrease in the partial concentration of ethylene at the surface, and the structure of the membrane increased the saturation time of the active sites and shifted the boundry toward higher pressures. When the number of incoming and transferred ethylene molecules (toward polymer active sites) moved close to each other, the possibility of accumulation in the active-layer structure lessened. Therefore, there was a higher number of unoccupied cation sites, and their saturation was posponed. A decrease in the salt molar concentration from 0.33 ([OH]/[Ag] = 3 : 1) to 0.25 ([OH]/[Ag] = 3 : 1) reduced the real selectivity from 6.8 to 4.6 at the lowest pressure. The other membranes did not show any selectivity in this experiment.

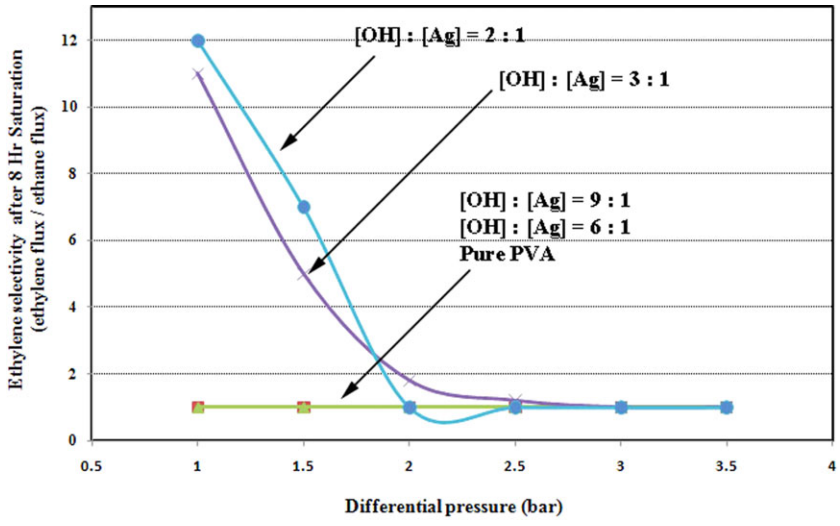

Figure 18. Ideal ethylene selectivity in PES/PVA/PDMS composite membranes containing different concentrations of silver nitrate after 8 h of saturation with an ethylene stream at 3.5 barg (PES = 18 wt %). [Color figure can be viewed in the online issue, which is available at www.interscience.wiley.com.]

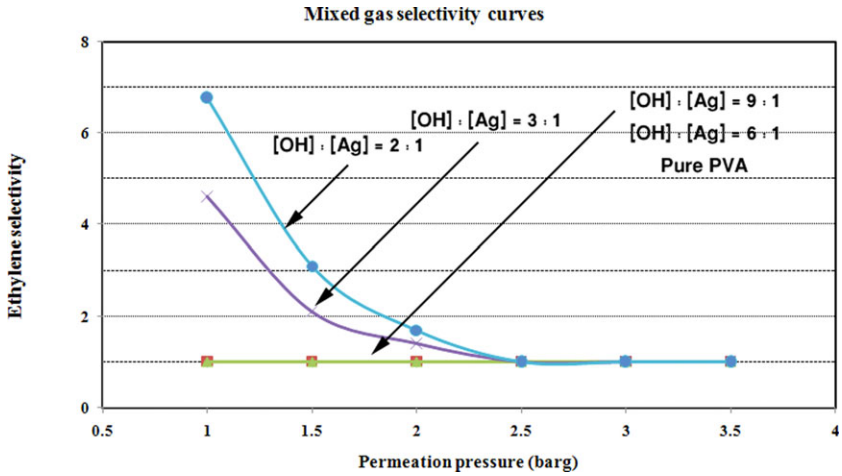

Figure 19. Mixed gas selectivity in the PES/PVA/PDMS composite membranes containing different concentrations of silver nitrate (feed composition = 50% ethylene and 50% ethane). [Color figure can be viewed in the online issue, which is available at www.interscience.wiley.com.]

The presence of a high lattice energy among ions of $AgNO_3$ salt prevented the effective and free distribution of silver cations among the polymer chains. The probability of aggregated ion distribution after the dissolution of metal salts with a high lattice energy was higher than that of other salts with low lattice energies. This phenomenon decreased the selectivity of the facilitated transport membranes because the heterogeneous and aggregated distributions disturbed the operation of the expected mechanism for olefin molecule transportation. The homogeneous and free distributions of ions in the membrane structure had an important effect on the efficiency of the facilitated transport mechanism. However, the existence of a highly electronegative element (oxygen) in the complex structure strongly attached the olefinic molecules to the silver cation ends of the complexes. The attached ethylene molecules needed a high driving force for jumping between active sites and transferring through the hopping mechanism. Therefore, the facilitated transport membranes prepared from $AgNO_3$ could not show a comparable performance toward the membranes containing salts with low lattice energies, such as $AgBF_4$ or $AgCF_3SO_3$. The mixture of silver nitrate salt with $AgBF_4$ or $AgCF_3SO_3$ is an effective method for improvement of selectivity. In this section, equimolar concentrations of $AgBF_4$ and $AgNO_3$ salts at four concentration levels were blended with each other and were used to improve the efficiency of ethylene transportation; the results are shown in Figure 20. In the best conditions, the real selectivity of the membrane containing the highest salt concentration increased from 6.7 to 33. The trend of selectivity variation, which was caused by the pressure and salt concentration variation, was the same as the latter case in which $AgBF_4$ was not applied. The addition of $AgBF_4$ enhanced the real selectivity of the membranes containing low salt concentrations ([OH]/[Ag] = 9 : 1 or 6 : 1) from 1 to 2.3 and 6.0 at a pressure of 1.0 barg. The potency of the facilitated transport mechanism increased after the addition of $AgBF_4$, with a lower lattice energy than $AgNO_3$. The better distribution of silver cations and the creation of weak complexes between the ethylene molecules and silver cations enhanced the membrane performance. The best

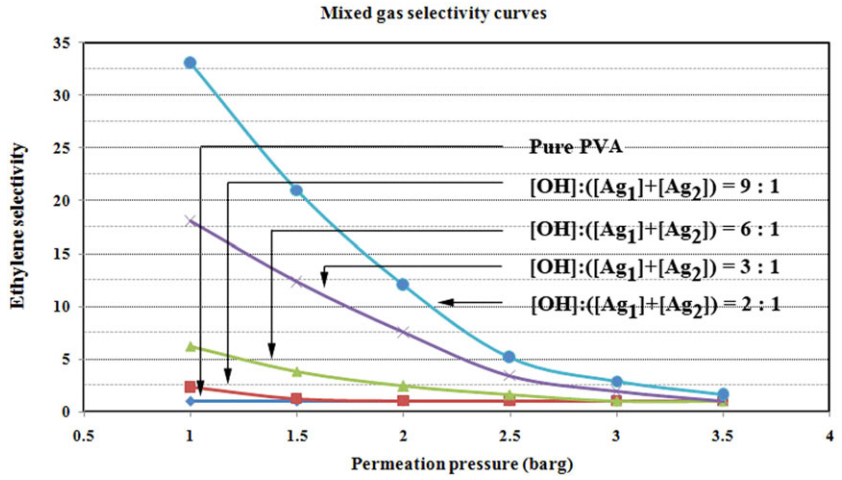

Figure 20. Mixed gas selectivity in the PES/PVA/PDMS composite membranes containing different concentrations of $AgNO_3$ and $AgBF_4$ (feed composition = 50% ethylene and 50% ethane). [Color figure can be viewed in the online issue, which is available at www.interscience.wiley.com.]

obtained selectivity by other researchers for propane/propylene separation by uncrosslinked PVA was near 3.0,[26] and there were not any reported results for ethylene/ethane separation with uncrosslinked PVA.

CONCLUSIONS

The increase in the silver salt concentration was associated with a weakening of the hydroxyl bonds, a decrease in the number of free hydroxyl sites, a fortification of the position of the carriers, and an enhancement of the distribution fluctuations of silver cations among the polymer chains. Variations of T_g of the silver-salt-containing membranes were accompanied by a higher structural disorder compared to that from crosslinking. The T_g values of the facilitated transport membranes shifted toward lower temperature regions through the salt-addition process. Salt addition caused the creation of a semicrystalline structure during the thermal process at temperatures higher than 160°C. Salt addition increased the membrane mechanical strength because of the increases in amorphism and free volume in the membrane structure. The surface roughness of the facilitated transport membranes cast on smoother support layers was greater than those of the other membranes with the same characteristics (and cast on rougher sublayers). The permeation rate, selectivity, and membrane active sites increased, and the effective distance between them decreased with increasing salt concentration. In this way, the performance of carrier agents in the membrane structure improved. On the other hand, the polymer amorphism and free volume increased with increasing salt concentration. Therefore, there was a greater potency for the permeation of gas molecules through a diffusion mechanism at higher operational pressures. The maximum ideal and real selectivities of the membrane containing the highest salt concentration were 31 and 6.7, respectively. The blending of $AgBF_4$ and $AgNO_3$ salts at each concentration level increased the real selectivity of the membranes. Under the best conditions, the real selectivity increased from 6.7 to 33 after salt blending.

ACKNOWLEDGMENTS

The authors gratefully acknowledge the financial support of this project by New Research Group, Petrochemical Research and Technology Co., Iran (contract grant number 0870288701).

REFERENCES

1. Deng, L.; Kim, T.J.; Hagg, M. B. *Desalination* **2006**, *199*, 523.
2. Mark, J. E. Polymer Data Handbook; Oxford University Press: Oxford, United Kingdom, **1999**.
3. Bolto, B.; Tran, T.; Hoang, M.; Xie, Z. *Prog. Polym. Sci.* **2009**, *34*, 969.
4. Deng, L.; Kim, T. J.; Hagg, M. B. *J. Membr. Sci.* **2009**, *340*, 154.
5. Pan, F.; Jia, H.; Jiang, Z.; Zheng, X.; Wang, J.; Cui, L. *J. Membr. Sci.* **2008**, *323*, 395.
6. Zhang, L. Z.; Wang, Y. Y.; Wang, C. L.; Xiang, H. *J. Membr. Sci.* **2008**, *308*, 198.
7. Guo, R.; Fang, Xin; Wu, H.; Jiang, Z. *J. Membr. Sci.* **2008**, *322*, 32.
8. Zhang, Z.; Ouriadov, A. V.; Willson, C.; Balcom. B. J. *J. Magn. Reson.* **2005**, *176*, 215.
9. Staudt-Bickel, C.; Koros, W. J. *J. Membr. Sci.* **1999**, *155*, 145.
10. Bai, S.; Sridhar, S.; Khan, A. A. *J. Membr. Sci.* **2000**, *174*, 67.
11. Kim, J. H.; Kim, C. K.; Won, J.; Kang, Y. S. *J. Membr. Sci.* **2005**, *250*, 207.
12. Mun, S. H.; Kang, S. W.; Cho, J. S.; Koh, S. K.; Kang, Y. S. *J. Membr. Sci.* **2009**, *332*, 1.
13. Yoon, Y.; Won, J.; Kang, Y. S. *Macromolecules* **2000**, *33*, 3185.
14. Hess, S.; Staudt-Bickel, C.; Lichtenthaler, R. N. *J. Membr. Sci.* **2006**, *275*, 52.
15. Pinnau, I.; Toy, L. G. *J. Membr. Sci.* **2001**, *184*, 39.
16. Koh, J. H.; Kang, S. W.; Park, J. T.; Seo, J. A.; Kim, J. H.; Kang, Y. S. *J. Membr. Sci.* **2009**, *339*, 49.
17. Shen, J.; Qiu, J.; Wu, L.; Gao, C. *Sep. Purif. Technol.* **2006**, *51*, 345.
18. Cussler, E. L.; Aris, R.; Bhown, A. *J. Membr. Sci.* **1989**, *43*, 149.
19. Noble, R. D. *J. Membr. Sci.* **1990**, *50*, 207.
20. Okabe, K.; Matsumiya, N.; Mano, H. *Sep. Purif. Technol.* **2007**, *57*, 242.
21. Matsuyama, H.; Terada, A.; Nakagawara, T.; Kitamura, Y.; Teramoto, M. *J. Membr. Sci.* **1999**, *163*, 221.
22. Yegani, R.; Hirozawa, H.; Teramoto, M.; Himei, H.; Okada, O.; Takigawa, T.; Ohmura, N.; Matsumiya, N.; Matsuyama, H. *J. Membr. Sci.* **2007**, *291*, 157.
23. Bryant, D. L.; Noble, R. D.; Koval, C. A. *J. Membr. Sci.* **1997**, *127*, 161.
24. Shen, J. N.; Wu, L. G.; Chen, H. L.; Gao, C. *J. Sep. Purif. Technol.* **2005**, *45*, 103.
25. Ho, W. S.; Dalrymple, D. C. *J. Membr. Sci.* **1994**, *91*, 13.
26. Kim, J. H.; Min, B. R.; Lee, K. B.; Won, J.; Kang, Y. S. *Chem. Commun.* **2002**, 2732.
27. Zidan, H. M. *Polym. Test* **1999**, *18*, 449.
28. Clemenson, S.; Alcouffe, P.; David, L.; Espuche, E. *Desalination* **2006**, *200*, 437.
29. Esmaeili, M.; Madaeni, S. S.; Barzin, J.; Yousefimehr, N. *Sep. Purif. Technol.* **2011**, *81*, 371.
30. Ha, K.; West, J. L. *Liq. Cryst.* **2004**, *31*, 753.
31. Reis, E.; Campos, F. S.; Lage, A. P.; Leite, R. C.; Heneine, L. G.; Vasconcelos, W. L.; Lobato, Z. I. P.; Mansur, H. S. *Mater. Res.* **2006**, *9*, 185.
32. Madaeni, S. S.; Esmaeili, M.; Barzin, J. *Polym. Polym. Compos.* **2007**, *15*, 579.
33. Esmaeili, M.; Madaeni, S. S.; Barzin, J. *Polym. Int.* **2010**, *59*, 1006.
34. Singh, S.; Khulbe, K. C.; Matsuura, T.; Ramamurthy, P. *J. Membr. Sci.* **1998**, *142*, 111.